EXPLORATION AND APPLICATION OF POST-INFRARED HIGH-TEMPERATURE INFRARED STIMULATED LUMINESCENCE DATING TECHNIQUES: INVESTIGATION OF MARINE TERRACE DEPOSITS ALONG THE NORTHERN SAN ANDREAS FAULT

by

JENNIFER ELIZABETH ROOZEBOOM

B.S., Kansas State University, 2011

A THESIS

submitted in partial fulfillment of the requirements for the degree

MASTER OF SCIENCE

Department of Geology
College of Arts and Sciences

KANSAS STATE UNIVERSITY
Manhattan, Kansas

2015

Approved by:

Major Professor
Dr. Joel Spencer

Copyright

Abstract

Optically stimulated luminescence (OSL) dating is a relatively new dating method, tangibly introduced in 1985 when Huntley et al. demonstrated the ability to use light-sensitive traps to measure radiation exposure and determine the age of sediment. Quartz and feldspar grains are commonly used for the method, with quartz receiving significantly more attention than feldspars until the past decade. Recent research has improved the practicality of using feldspars as a reliable dosimeter –an appealing notion as the intrinsic properties of feldspars allow them to date older sediment that may lie beyond the reliable range of quartz dosimetry. This work explores and utilizes the contemporary feldspar technique termed post-infrared, high-temperature infrared stimulated luminescence (pIRIR) dating to add to the existing knowledge base of this method, particularly by testing different preheat and measurement temperature combinations. Analysis of the each pIRIR method indicates that the pIRIR signal stimulated at 225°C is more appropriate for dating than the pIRIR signal stimulated at 290°C. Techniques and protocols developed in this work are done so via their application to a marine terrace that is displaced by the San Andreas Fault. Corals from the terrace along the Pacific plate, dated with U-series by Muhs et al. (2002), offer an age estimate. Comparison of the pIRIR ages to the U-series ages yield an underestimation, suggesting the pIRIR method may be more useful as a means of correlating terraces across the fault, than for providing ages of terrace formation.

Huntley, D.J., Godfrey-Smith, D.I., Thewalt, M.L.W., 1985. Optical dating of sediments. Nature 313, 105-07.

Muhs, D.R., Simmons, K.R., Kennedy, G.L., Ludwig, K.R., and Groves, L.T., 2002. A cool eastern Pacific Ocean at the close of the last interglacial period, ca. 80,000 yr B.P. Geological Society of America Abstracts with Programs, 34, 130.

Table of Contents

List of Figures

List of Tables

Acknowledgements

Thanks to the supporters of this work: the GSA Research Grant, KSU Geology Department, Geology Alumni, KSU Graduate Student Council, Kansas Geological Foundation, United States Geological Survey (USGS), and a special thanks to the KSU OSL Laboratory, where all preparation and measurements were carried out.

Thanks very much to my major professor Joel Spencer, for providing excellent guidance throughout this work, endless edits for papers and presentations, conducting fieldwork with me, co-authoring my manuscript, finding time to help me when he had none, and saying funny words. Thanks also to my committee members, Jack Oviatt and Matt Kirk, and my department head Pamela Kempton, for additional comments and edits, and helping me thoroughly think through concepts.

Special thanks to my other manuscript co-authors Carol Prentice and Steve DeLong, USGS, who also conducted field work with me, and organized special access for sampling on private property. Thanks to the other USGS editors who provided additional comments and edits.

Big thanks to Sébastian Huot, for providing a fading template, along with quick and personal help in using it.

Thanks to my husband Andrew, for making me many sandwiches and gallons of tea as I pursued this degree.

Dedication

This thesis is dedicated to my mother, who spent her every breath encouraging others.

Chapter 1 - Introduction

Brief History

Optically stimulated luminescence (OSL) dating is a relatively new dating method, the potential for which was realized while developing techniques for a similar and related method: thermoluminescence (TL) dating. In 1985, Huntley, Godfrey-Smith & Thewalt presented the pilot work by demonstrating how light-sensitive traps, that are difficult to accurately assess with TL approaches, can be readily used to measure the radiation exposure during burial to determine the age of sediments via OSL (Huntley et al., 1985). Since this founding work, many studies have advanced the method; most notably, the development of the single-aliquot regenerative-dose (SAR) protocol for quartz (Murray & Wintle 2000, 2003; Wintle & Murray, 2006), which provided an analytical approach to measurement that significantly improved the accuracy and precision of results.

Since 1985, quartz has been the main focus of OSL research, and has been determined to be a reliable dosimeter (e.g. Murray and Olley, 2002; Rittenour, 2008). However, as techniques were improved, limitations were also recognized. Though quartz is nearly ubiquitous on Earth's surface, there are some places, like Hawaii and Iceland (due to predominately mafic volcanic origins), that are nearly devoid of this mineral (Thomsen et al. 2008). Quartz present in glacial sediments may have been poorly exposed during transport or subaerial weathering, and may have undergone rapid deposition, and thus could be insufficiently bleached (Fuchs and Owen, 2008; Spencer and Owen, 2004;); they therefore tend to yield an age overestimation (Duller et al. 2005). Lukas et al. (2007) also encountered glaciogenic sediment with weak or absent fast components, which is the portion of the luminescence signal that is most adequately bleached in the natural environment. Similarly, quartz that has been recently eroded from bedrock has

potentially not been well exposed, and will also have low sensitivity to measurements (Rhodes, 2011). Additionally, quartz is not typically used for dating beyond ca. 200 ka due to the saturation of the mineral (Thiel et al., 2011). It is for these reasons and others that feldspars are gaining more attention. Having a second mineral to examine increases the suitability of OSL in different environments. Though Spencer and Owen (2004) indicated feldspars might also exhibit insufficient bleaching in glacial environments, feldspars are generally thought to be more sensitive than quartz (Hütt et al., 1988; Thomsen et al., 2008), implying fewer feldspar grains are needed to produce a bright signal. Perhaps most alluring, though, is the widely accepted theory that feldspars do not saturate as early as quartz minerals do, having luminescence signals that can grow to larger doses, and thus can be used to date older sediment (Rhodes, 2011; Thomsen et al. 2008; Thiel et al., 2011; Roberts, 2012; Auclair et al. 2003).

Though feldspars may provide an alternative to some of the quartz limitations, they also present a significant obstacle of their own: the unpredictable loss of charge that results in an underestimation in age. In 1973, prompted by unsuccessful attempts to use feldspars to date lava flows via TL, A.G. Wintle decided to test the stability of the TL signal in feldspars (and other minerals). She observed a reduction in the TL glow curve with time, and deduced that feldspars lost charge carriers from specific traps, terming this phenomenon “anomalous fading” (Wintle, 1973). In 1988, Hütt, Jaek, and Tchonka demonstrated that potassium feldspars are sensitive to infrared stimulation (Hütt et al., 1988), showing potential for targeting feldspars alone. However, N.A. Spooner (1992, 1994) later showed anomalous fading in the OSL and IRSL signal of feldspars. Though the potential for feldspars was realized early, the focus of the work has largely been devoted to developing corrections for anomalous fading. To that end, a significant discovery by Thomsen et al. (2008) was made which suggested that measuring feldspar IRSL

signals at elevated temperatures after a prior IR stimulation could reduce the need to correct for anomalous fading. This technique was later termed post-infrared high-temperature infrared stimulated luminescence (pIRIR), and Thomsen's work opened the door to subsequent and current research dedicated to exploring different preheat and measurement temperature combinations. Of these, and of particular interest to this thesis, are the studies of different pIRIR approaches conducted by Thomsen et al. (2008, 2011) and Thiel et al. (2011), on which preheat and measurement temperatures for this work are based.

Foundational Concepts

The basis for OSL is that as sediment is buried, intrinsic and environmental radiation ionizes charge that can be trapped in the lattice defects of certain silicate minerals. Whether in whole rock formations, or as unlithified sediment, these mineral grains accumulate charge and increase energy over time. If sediment grains are exposed to natural daylight at deposition, the energy from solar exposure is sufficient to evict accumulated charge, which in turn can recombine at lower energy states with the release of a small amount of energy as a luminescence signal, effectively resetting or "zeroing" the dating clock. The amount of environmental radiation exposure is proportional to the intensity of the luminescence signal, which in turn is proportional to age since daylight resetting. In a laboratory setting, luminescence signals are measured from the silicate minerals by optically stimulating the trapped charge using light emitting diodes and a sensitive photomultiplier tube (PMT) light detector. The natural radiation dose is measured by calibrating the natural luminescence with luminescence from regenerated lab doses to form a growth curve. Age is calculated by combining the natural radiation dose with environmental dose-rate information. The latter can be obtained using a variety of methods to measure either

natural radioactivity or elemental concentration data, which are converted to dose-rate information using well-established conversion factors.

This Thesis

This research is an exploration of pIRIR techniques using modified SAR protocols on feldspar minerals (Thomsen et al., 2008, 2011; Thiel et al., 2011). The specific luminescence properties of feldspar minerals require measuring protocols distinct from those more routine SAR approaches developed for quartz. As such, two alternative temperature protocols were analyzed based on a comparison of the results for various tests. The techniques and methods developed were applied as an assessment of sediment mantling on a marine terrace, which is exposed at various locations along the coast of northern California. The terrace has undergone regional uplift, and been offset by the San Andreas Fault (SAF) in the late Quaternary, thereby providing a method of calculating late Quaternary slip rates for the fault. Muhs (2002) provided an age of ca. 80,000 yr B.P. for corals found on the terrace using U-series dating. If in situ, these would also yield an age for the terrace itself. The manuscript presented in Chapter 2 of this thesis is an investigation of these relationships, with the following two objectives: 1) explore and apply the pIRIR method to provide sediment ages comparable to existing U-series coral ages; 2) correlate the terrace across the SAF by providing corresponding ages for sediment on each side. Chapter 3 reiterates manuscript conclusions within the context of a comprehensive summary; and, the appendices provide radial plots and growth curves pertaining to individual measurements made throughout this research.

Chapter 2 - Manuscript

EXPLORATION AND APPLICATION OF pIRIR DATING TECHNIQUES TO INVESTIGATE MARINE TERRACE DEPOSITS ALONG THE NORTHER SAN ANDREAS FAULT

Roozeboom, Jennifer E.[1*], Spencer, Joel Q.G.[1], Prentice, Carol S.[2], DeLong, Stephen B.[2]

[1]*Department of Geology - Kansas State University, Manhattan, KS 66502, USA*
[2]*US Geological Survey - 345 Middlefield Rd MS 977, Menlo Park, CA 94025, USA*
[*]*Corresponding author: jboswell@ksu.edu*

Key words: optically stimulated luminescence, pIRIR, feldspars, San Andreas fault, marine terrace

Abstract

Late Quaternary slip rates for the northern San Andreas Fault (SAF) have been calculated, but are dependent upon the accuracy of the ages and the correlation of geomorphic features across the fault. U-series analyses of coral from two exposures of sediment mantling the lowest extensive marine terrace along the northern California coast – the Point Arena (PTA-) terrace – suggest an age of ~80 yr B.P., which is consistent with marine oxygen isotope substage 5a chronology. Earlier work using the single-aliquot regenerative-dose (SAR) approach with quartz suggest that either the Optically Stimulated Luminescence (OSL) may have reached dose-saturation levels, or was poorly bleached prior to deposition, giving discordant results compared to U-series ages. The post-infrared high-temperature infrared stimulated luminescence (pIRIR) technique for feldspars has been shown to produce accurate ages up to 600 ka and in suitable low-dose environments, up to ~1 Ma. We investigate an alternative luminescence dating

approach, the pIRIR dating of potassium-rich feldspar minerals using SAR protocols, to correlate the PTA-terrace across the San Andreas Fault and test previously estimated Quaternary slip rates. Ratios from dose-recovery tests that are close to unity indicate a $pIRIR_{225}$ measurement, with 250°C 60-s preheat, is the most appropriate approach. Our luminescence data, including assessment of fading, residual dose levels and preliminary ages for marine terrace deposits may provide a technique for correlating marine terraces along the northern California coast.

Introduction

The San Andreas Fault (SAF) system dissects California with the North American plate to the NE, and the Pacific plate to the SW. Regional uplift and right-lateral movement is exposing and displacing Quaternary marine terraces along the California coast. Correlating geomorphic features across the SAF can provide valuable information about past fault motion and serve as a foundation for assessing future potential hazards. Slip rates are important for infrastructure design of pipelines, roads, railroad tracks, and bridges in areas near to, or that overlie, active fault systems. Previous work by Prentice (1989) investigated Holocene and Pleistocene slip rates of the SAF north of San Francisco. In observing the displacement of a buried Holocene river channel near Point Arena (Fig. 2.1) and a late Pleistocene landslide (~40 miles, or ~65 km, south of Point Arena along the coast), and obtaining radiocarbon dates of charcoal from each feature, Prentice calculated slip rates of 25.5 ± 2.5 mm/yr and a maximum of ~39 mm/yr, respectively. Prentice also noted the lateral displacement of five marine terraces in the Point Arena area using their relative geomorphic position and elevation. Using a single U-series age and assuming terrace formation during high-sea-level stands, Prentice calculated another late Pleistocene slip rate of about 18-19 mm/yr from the offset of the two lowest terraces. The lowest terrace in her work (Terrace 1) is later identified as the Point Arena terrace (Muhs et

al. 2003) and is the terrace studied in this work, hereafter abbreviated to PTA-terrace. Prentice and Kelson (2006) refined the mapping of the PTA-terrace across the SAF using LiDAR, during which a 1.3 - 1.8 km offset was observed (Fig. 2.2). Figure 2.1 shows the location of sampling sites for the present study: Point Arena (PTA), Green Oaks Creek (GOC) on the Pacific plate, and Mendocino (MEND) on the North American plate. All sampling sites are assumed to be along the PTA-terrace. U-series analysis of a single Balanophyllia coral from the PTA-terrace at Point Arena yielded an age of 83,000 ± 800 yr B.P. (Muhs et al, 2002). In the same study, additional U-series analyses of eleven corals at Green Oaks Creek from the PTA-terrace gave rise to ages ranging from 75,800 ± 800 to 84,000 ± 600 yr B.P. The strong agreement of these ages support the correlation of this terrace between the Pacific plate locations, and are broadly consistent with the marine oxygen isotope substage 5a, suggesting that they were cut during the 80,000 yr B.P. high stand.

In 2008, samples from three locations on the Pacific plate (Fig. 2.1); GOC, Tomales Bay (TP), and PTA, were taken for optically stimulated luminescence (OSL) dating of quartz minerals. Preliminary results from these data give ages that are underestimated when compared to the U-series ages. Some of the data suggest that the quartz luminescence may have reached dose-saturation levels, and scatter in the data suggest that some of the grains were poorly bleached prior to deposition. This interpretation suggests an alternative OSL approach should be considered. The post-infrared high-temperature infrared stimulated luminescence (pIRIR) technique for feldspars has been shown to produce accurate ages up to 600 ka, and in suitable low-dose environments, up to approximately 1 Ma (Buylaert et al. 2012). Also, the initial infrared and high temperature treatments of this technique significantly reduce problems of unstable feldspar signals.

Figure 2.1 Map of coastal central-northern California showing location of sampling sites (diamonds) and other locations mentioned in the text (circles).

The problems addressed in this project are two-fold: prior OSL dating of offset marine terraces on the northern SAF has potentially been hindered by technical limitations, such as the early saturation of quartz minerals (Grove et al., 2010; Spencer et al., unpublished); and, correlation of marine terraces across the SAF are needed to add confidence to previous dating and mapping work. In addressing these core objectives, this project provides further validation of correlative terraces across the SAF, which also validates slip rates by extension; as well as

providing additional data to enhance and test the pIRIR luminescence dating method for feldspars.

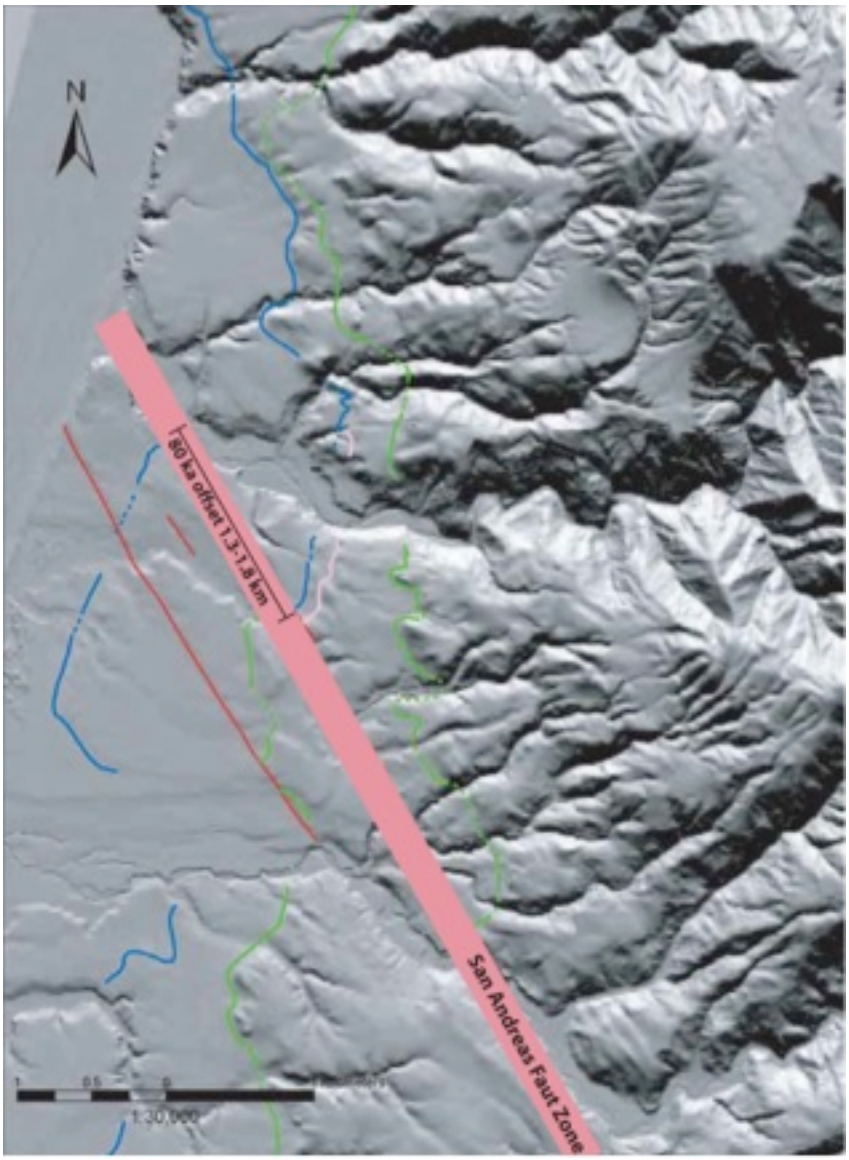

Figure 2.2 LiDAR image showing lateral offset of the Point Arena marine terrace (blue), and older terraces (pink and green) across the San Andreas Fault, as determined by geomorphic relationships. Red lines represent splays of the San Andreas Fault. Modified from Prentice and Kelson (2006).

Study Area

Sites were sampled in 2008 and 2010; Mendocino sites were sampled in 2010. In 2014, we returned to sites previously sampled in 2008 and 2010 to collect additional material to replicate and compare prior sampling and dosimetry data. The GOC and PTA sampling sites are both bound by the SAF on the east, and by the Pacific Ocean on the west. They are southwest of the SAF, and are located on the Pacific plate. Mendocino (MEND) sampling sites are north of the SAF, and are located on the North America plate (Figure 2.1). Multiple samples from each site were taken, and for this project three samples from PTA, three samples from GOC, and one sample from MEND were analyzed to determine the age of the sediments.

Point Arena

Three samples were taken from two locations at PTA. PTA-01 (2008), and PTA-06 (2014) were gathered ~0.51 m above the platform in gently cross-bedded sands; altitude ~26 m, overburden ~10 m, (GPS: 38.95445N, 123.73741W). From sieve fractions (discussed more in Methods), the mode of the sand distribution for PTA-01 falls between 125 and 250 μm, and for PTA-06 falls between 175 and 250 μm, indicating these are fine sands. Sediment from the 175 to 212 μm fraction was processed for measurement for both samples. Sample PTA-02 (2008) was taken from sands ~1 m above the terrace platform, and situated between two gravel layers; altitude ~26 m, overburden ~4.1 m, (GPS: 38.93335N, 123.72576W). The mode of the sand distribution from this location also indicates fine sands, and sediment from the 175 to 212 μm fraction was processed for measurement.

Green Oaks Creek

Three samples were taken from two locations at GOC. For samples GOC-01 (2008) and GOC-02 (2008) we sampled ~0.45 m above a prominent marine fossil layer, ~1 m above the

platform, altitude ~9 m overburden ~5 m, (GPS: 37.13217N 122.33725W) (Fig. 2.3). The mode of the sand distribution at these two locations falls between 90 and 212 μm, and indicates very fine to fine sands. Sediments processed for measurement of GOC-01 and GOC-02 were from the 175 to 212 μm fraction. Sample GOC-10 (2014) was taken ~0.55 m above the terrace platform from a sand lens within the marine fossil layer; altitude ~9 m, overburden ~5.8 m, (GPS: 37.13217N, 122.33725W). The distribution of sieve fractions indicate these sands are predominantly fine sand, with nearly 60% of sieved portion falling between 125 to 175 μm. Sediment from the 125 to 175 μm fraction was processed for measurement of GOC-10.

Mendocino

One sample (MEND-06) was processed from Mendocino. Sample MEND-06 was taken ~0.5 m above the terrace platform; altitude ~15 m, ~12 m overburden, (GPS: 39.30508N and 123.81033W). Before sampling, sands at this site were significantly cut back to avoid bioturbated areas, though some iron oxide staining was still present during sampling. The mode of the sand distribution falls between 212 to 500 μm, suggesting these are fine to medium sands. Sediment from the 212 to 250 μm fraction was processed for measurement.

Terrace Deposits

Tectonic uplift plays a significant role in preserving marine terraces, as a rising coastline is necessary to remove wave-cut platforms from the active erosional area (Prentice, 1989; Muhs et al., 2003; Grove et al., 2010). A progressive five-stage model for marine terrace formation and sediment deposition along the coast of central California is presented by Bradley and Griggs (1976), and discussed here in the same manner. Their diagrammatic sketch is reproduced here as Figure 2.4. As sea level rises rapidly (assumed in this study to be in response to melting glaciers and the beginning of an interglaciation), eustatic changes greatly exceed the rate of coastal uplift

and land is submerged (stage 1). As the rise in sea level begins to slow, and the eustatic change only slightly exceeds the rate of coastal uplift, the waves begin to cut and shape the terrace platform (stage 2). By stage 3, the rise in sea level and coastal uplift rates are balanced, and thus the affects of each are cancelled and a high sea stand persists.

At this time, fine sediment in the suspended load is transported seaward, and coarse sediment and the bedload undergo longshore transport toward Monterey Bay. Erosion is at a maximum and continues to cut the platform until (stage 4) the platform gradient is made low enough to dissipate the wave energy necessary to maintain lateral transport. Sea level begins to slowly drop as coastal uplift persists, during which beach progradation is occurring due to the deposition of sediment that is no longer laterally transported. During stage 5, sea level begins to fall rapidly and the landward edge of the platform is abandoned by regression, and preserved by uplift. It is typical for alluvial –colluvial deposits to overlie marine deposits (Prentice, 1989) but it is assumed that the origin of the sediments studied presently is marine. For clarity, a detailed sedimentology study is recommended and implications are discussed below.

Figure 2.3 Sampling of GOC-01, approximately 0.45 m above the fossil layer, and approximately 1 m above the platform.

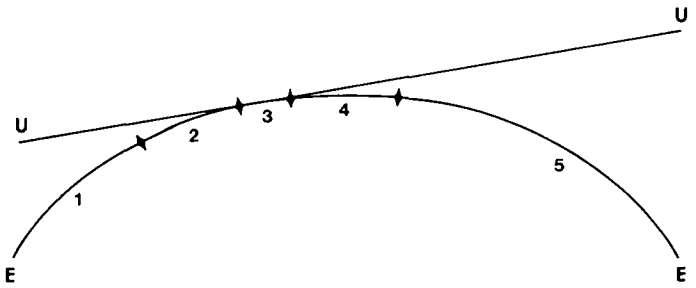

Figure 2.4 Diagrammatic sketch illustrating the relationship between uplift (U) and eustatic sea-level (E) during interglacial highstands over time. Stages 1 to 5 are discussed in the text. From Bradley and Griggs (1976).

Methods

Preparation and Instrumentation

Samples were collected using light-tight metal cylinders, the ends of which were sealed with duct tape after being hammered into and excavated from cleaned sections. At Kansas State University, the samples were opened and prepared under very low intensity amber lighting. Cylinder ends (~2-3 cm) were removed as this portion may have been exposed to light during sampling, and were often used for dose-rate analysis. All sediment was dried in a 50°C oven to record field moisture, and ~100 g of interior sediment was sieved through a tower separated by meshes of 90, 125, 175, 212, 250, and 500 μm in size to isolate discrete grain-size fractions. Interior sediment, ranging in grain size from 125-175 μm, 175-212 μm, or 212-250 μm was treated with 10% hydrochloric acid and 30% hydrogen peroxide to remove carbonates and organic matter, respectively. The potassium-rich feldspar fraction was isolated using 2.58g/cm^3 lithium metatungstate, and was loaded onto 10 mm diameter stainless steel discs as 3mm diameter mono-layered circles. All luminescence measurements were made using an automated Risø TL/OSL reader equipped with a ^{90}Sr/^{90}Y beta source delivering approximately 0.14 Gy/s,

and infra-red LEDs. Signals were detected in the near-UV to blue spectral range through 2 mm Schott BG-39 and 4 mm Corning 7-59 filters with an EMI 9235QB photomultiplier tube.

Environmental Dose Rate

Dosimetry data for each site are shown in Table 2.1. Approximately 20 mL of dried sample was pulverized into a fine powder using a tungsten carbide ring and puck mill within a shatter box. About 3 g of the crushed material from about half of the samples were sent to Activation Laboratories (ActLabs) in Ontario, Canada, for inductively coupled plasma mass spectrometry (ICP-MS) and inductively coupled plasma optical emission spectrometry (ICP-OES) to determine the elemental concentrations of U, Th, K (Table 1) and Rb. Elemental concentrations were determined for the rest of the samples using on-site gamma spectroscopy. Internal potassium was assumed to be 12.5% ± 0.5% after Huntley and Baril (1997). To calculate beta and gamma dose-rate components, conversion factors from Adamiec and Aitken (1998), and beta attenuation factors from Rainer Grün's "Age" program were applied. Cosmic ray dose-rate components were estimated using the depth to each sample, and according to Prescott and Hutton (1994). Water content was determined using the mass of the sample when first opened, and the mass of the sample after drying in a 50°C oven.

Table 2.1 Summary of the dosimetry data.

Sample	Depth (m)	U[a] (ppm)	Th[a] (ppm)	K[a] (%)	Cosmic dose-rate[b] (Gy/ka)	Total dose-rate (Gy/ka)
GOC-01	5.2	1.34 ± 0.13	4.12 ± 0.21	1.33 ± 0.07	0.11 ± 0.005	2.73 ± 0.17
GOC-02	5.2	1.34 ± 0.13	4.12 ± 0.21	1.33 ± 0.07	0.11 ± 0.005	2.73 ± 0.17
GOC-10	5.8	1.34 ± 0.05	3.53 ± 0.10	1.14 ± 0.01	0.10 ± 0.005	2.27 ± 0.11
PTA-01	7.8	1.57 ± 0.16	4.40 ± 0.22	1.72 ± 0.09	0.08 ± 0.004	3.24 ± 0.15
PTA-02	4.1	1.44 ± 0.14	4.25 ± 0.21	1.68 ± 0.08	0.12 ± 0.006	3.03 ± 0.18
PTA-06	7.8	1.57 ± 0.16	4.40 ± 0.22	1.72 ± 0.09	0.08 ± 0.004	3.24 ± 0.15
MEND-06	4.0	0.78 ± 0.03	2.45 ± 0.07	0.87 ± 0.01	0.12 ± 0.006	2.05 ± 0.07

[a]Elemental concentrations from ActLabs, Ontario, CA for samples GOC-01, GOC-02, PTA-01, PTA-02; elemental concentrations for samples GOC-10, and MEND-06 from on-site gamma spectroscopy. Conversions based on Adamiec and Aitken (1998), and Rainer Grün's "Age" program.
[b]Estimations according to Prescott and Hutton (1994).

Infrared Stimulated Luminescence (IRSL) Measurements

All equivalent dose values (D_e) were obtained using the single-aliquot regenerative-dose (SAR) protocol (Murray & Wintle, 2000; Wintle & Murray, 2006) modified for post-IR IRSL with different preheat and measurement temperatures adopted from Thomsen et al. (2008, 2011) and Thiel et al. (2011), outlined in Table 2.2 (modified from Thiel et al., 2011). The structure of each protocol is the same: measurement of the natural dose or regenerative dose (step 1), preheat (steps 2 and 6), IR stimulation (steps 3 and 7), another IR stimulation- i.e. the pIRIR- (steps 4 and 8), a constant test dose (step 5) and a hotbleach (step 9). Steps 5 through 8 comprise the luminescence sensitivity correction. The hotbleach is incorporated at the end of each cycle to minimize residual charge before any subsequent regenerative dose is given. The preheat is designed to evict unstable charge from crystalline defects, as higher temperatures evict charge from deeper traps and thus adds stability to remaining luminescence signal. However, deeper traps are more difficult to evict charge from (as they require higher temperatures to do so) and may also be more difficult to bleach in the natural environment. In general, the preheat

temperature should be higher than the pIRIR stimulation, and the hotbleach temperature should be higher than the preheat temperature (Roberts, 2012). The changes in protocol were made to the temperatures and duration of the preheat, pIRIR, and hotbleach. The test dose for each protocol is ~21 Gy. Equivalent dose values (D_e) were calculated using the initial 4 s of the $pIRIR_{290}$ signal, and the initial 2 s of the $pIRIR_{225}$ signal, from which background signals were subtracted as determined by the final 20 and final 10 seconds of the decay curve, respectively. Figure 2.5 demonstrates a SAR growth curve where the x-axis is the regenerative dose, and the y-axis represents the sensitivity-corrected IRSL signal. Each regenerative dose corresponds to another point on the growth curve, and the natural dose plots on the y-axis. Using the growth curve, the natural dose is projected onto the x-axis, and an equivalent dose is interpolated.

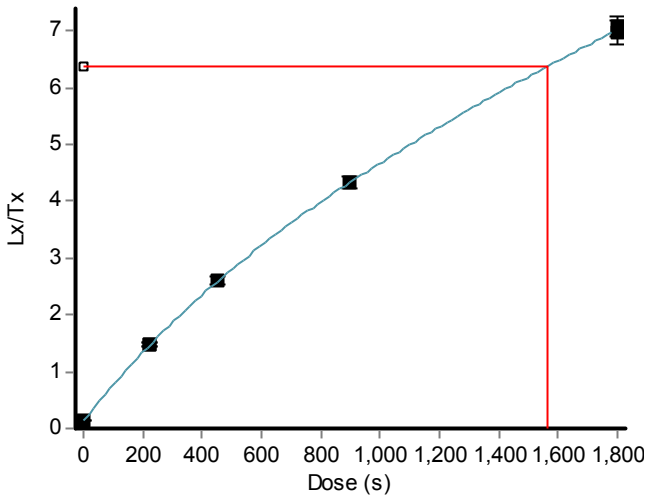

Figure 2.5 Growth curve for PTA-02 measured with the $pIRIR_{290}$ protocol. The x-axis is the regenerative dose in seconds, and the y-axis is the net sensitivity corrected IRSL. The natural dose plots on the y-axis, and is interpolated to the x-axis via the growth curve to give the estimated equivalent dose (D_e).

Table 2.2 Post-IR IRSL (pIRIR) sequences for each preheat and measurement temperature combination. $pIRIR_{225}$ modified from Thomsen et al. (2008, 2011); $pIRIR_{290}$ modified from Thiel et al. (2011).

Step	Treatment = $pIRIR_{225}$	Treatment = $pIRIR_{290}$
1	Regenerative dose	Regenerative dose
2	Preheat: 60 seconds at 250 °C	Preheat: 60 seconds at 320 °C
3	IR stimulation: 100 seconds at 50 °C	IR stimulation: 200 seconds at 50 °C
4	IR stimulation: 100 seconds at 225 °C	IR stimulation: 200 seconds at 290 °C
5	Test dose	Test dose
6	Preheat: 60 seconds at 250 °C	Preheat: 60 seconds at 320 °C
7	IR stimulation: 100 seconds at 50 °C	IR stimulation: 200 seconds at 50 °C
8	IR stimulation: 100 seconds at 225 °C	IR stimulation: 200 seconds at 290 °C
9	IR stimulation: 40 seconds at 290 °C	IR stimulation: 40 seconds at 325 °C

The first temperature protocol applied in this study was developed by Thiel et al. (2011), based on the observation of Murray et al. (2009) who demonstrated that temperatures as high as 320°C do not erode the main dosimetry traps in coarse-grained potassium-rich feldspars (though Roberts, 2012, demonstrated this protocol was inappropriate for the dating of her samples). The protocol involves a preheat temperature of 320°C for 60 s, IR stimulation at 50°C for 200 s, pIRIR stimulation at 290°C for 200 s, and a hotbleach at 325°C for 100 s . For the present study, the hotbleach was a duration of 40 s, with all other parameters the same.

The second temperature protocol applied in this study was developed by Thomsen et al. (2008, 2011), and included a preheat temperature of 250°C for 60 s, IR stimulation at 50°C for 100 s, pIRIR stimulation at 225°C for 100 s, and according to Thomsen et al. (2011) a hotbleach at 330°C for 100 s, though the present study used a hotbleach at 290°C for 40 s.

Results

The following results are from those samples with recycling ratios within ± 10% of unity, and with dose response curves that pass through the origin, unless otherwise noted. Ages were determined using a central age model (Galbraith et al., 1999); residual levels were subtracted where applicable, and fading rates assessed.

Residual dose levels

To determine sample bleachability, residual dose tests were conducted. Aliquots were not given a laboratory dose before measurement, and values with errors are an average (for most, n=2). Numerical results are tabulated in Table 2.3, and spatial relationships between protocols are shown in Figure 2.6.

Table 2.3 Residual dose levels for the $pIRIR_{225}$ and $pIRIR_{290}$ protocols.

Sample	$pIRIR_{225}$ (Gy)	$pIRIR_{290}$ (Gy)
PTA-02	18.13 ± 0.56	25.12 ± 0.84
GOC-01	4.67 ± 0.14	11.17 ± 0.38
GOC-10	7.74 ± 0.48	
MEND-06	58.59 ± 36.62	

Higher temperature protocol: $pIRIR_{290}$

Four aliquots of PTA-02 and GOC-01 were set on a windowsill for three sunny days, and divided between the measuring protocols outlined in Table 2.2 ($pIRIR_{225}$ results below). Residual dose levels calculated using the $pIRIR_{290}$ gave a value of 25.12 ± 0.84 Gy for PTA-02, and a value of 11.17 ± 0.38 Gy for GOC-01 (Table 2.3; Fig. 2.6).

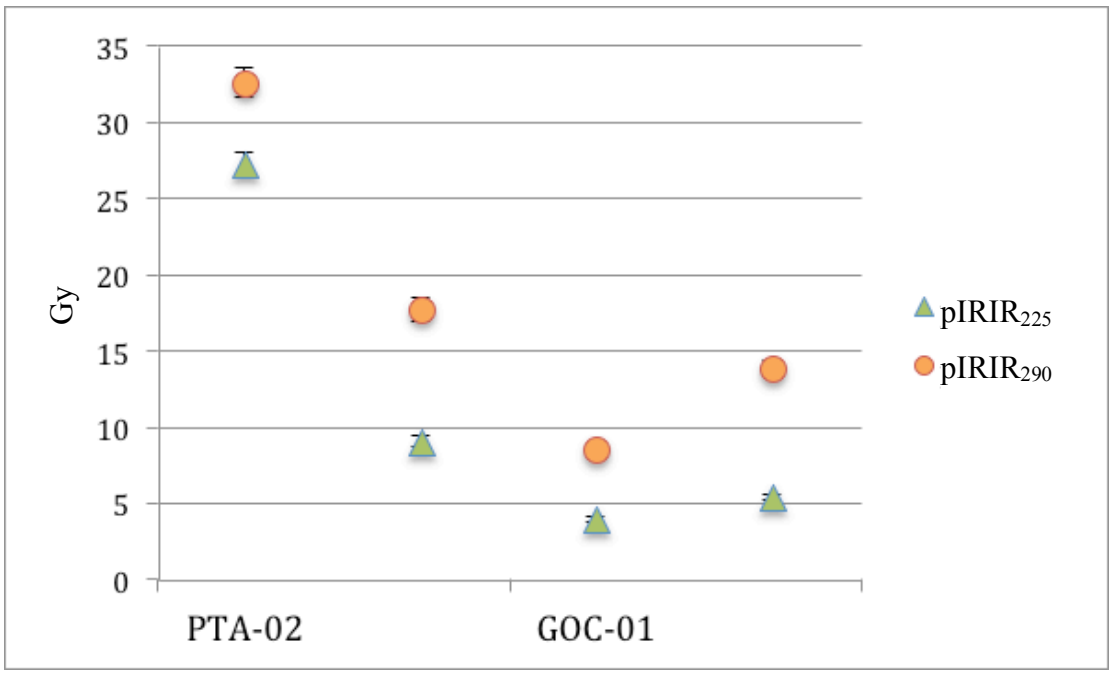

Figure 2.6 Residual dose levels of $pIRIR_{225}$ and $pIRIR_{290}$ demonstrating spatial relationship between protocols for PTA-02 and GOC-01. Each point represents a single aliquot that was bleached for 3 sunny days; errors are confined within the data points.

Lower temperature protocol: $pIRIR_{225}$

In addition to the two aliquots of PTA-02 and GOC-01, two aliquots of GOC-10 and two aliquots of MEND-06 were bleached on a sunny windowsill for 24 h; all were measured using the $pIRIR_{225}$ (Figs. 2.6 & 2.7). Residual dose levels for PTA-02, GOC-01, and GOC-10 are 18.13 ± 0.56 Gy, 4.67 ± 0.14 Gy, and 7.74 ± 0.48 Gy, respectively (Table 2.3). The residual dose level for MEND-06 is an average of 58.59 ± 36.6 Gy, calculated from five aliquots. This value is large, with an unacceptably high error (Fig. 2.7a), and thus is not included when determining the best age for MEND-06.

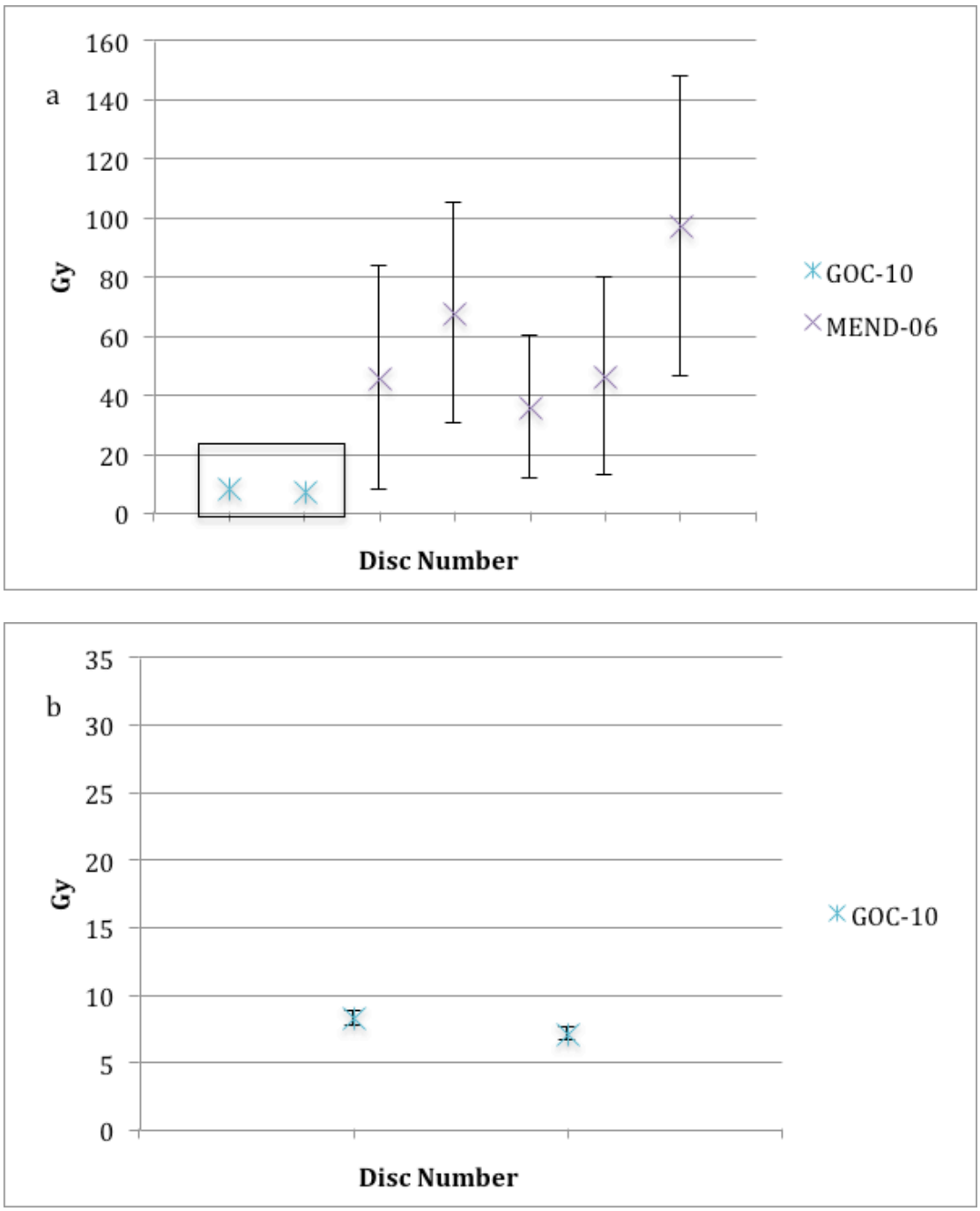

Figure 2.7 a) Summary of residual dose levels from $pIRIR_{225}$ for samples GOC-10 and MEND-06. Each point represents a single aliquot that was bleached for 24 h. Note the vertical scale; black box is replicated as (b). b). Residual dose levels from $pIRIR_{225}$ for sample GOC-10. Errors not confined within data points are represented with bars.

Fading rates

To assess the fading of the $pIRIR_{225}$ protocol, fading tests of the IR signal at 50ºC and the post-IR IRSL at 225ºC were conducted using prompt delays, following Auclair (2003), and compiled into Excel macros from Sébastian Huot in A Recipe Book For Fading. Samples GOC-10 and MEND-06, from which the natural dose was previously measured, were selected for these tests, results shown in Table 2.4.

IR signal at 50°C

The fading rate for GOC-10 from the IR_{50} signal is 5.6 ± 1.1 %/decade; the fading rate for MEND-06 from the IR_{50} signal is 4.9 ± 0.9 %/decade (Table 2.4). Since these values are significant, ages calculated from these signals should be corrected for fading. The fading corrected age from this signal for GOC-10 is 52.42 ± 4.33 ka, and for MEND-06 is 43.85 ± 16.25 ka (Table 2.4).

Post-IR IRSL signal at 225°C

The fading rate for GOC-10 from the $pIRIR_{225}$ signal is 1.8 ± 1.1 %/decade; the fading rate for MEND-06 from the $pIRIR_{225}$ signal is 2.1 ± 1.0 %/decade (Table 2.4). Ages calculated with fading rates are shown in Table 2.6; however, since these rates are rendered nearly obsolete within errors, fading rates are not applied to the final, or best, age.

Sample	D_e (Gy)		G-value (%/decade)		Fading corrected ages (ka)
	IRSL at 50ºC	Post-IR IRSL at 225ºC	IRSL at 50ºC	Post-IR IRSL at 225ºC	IRSL at 50ºC
GOC-10	118.92 ± 8.09	123.91 ± 6.63	5.6 ± 1.1	1.8 ± 1.1	52.42 ± 4.33
MEND-06	90.01 ± 33.20	133.86 ± 5.15	4.9 ± 0.9	2.1 ± 1.0	43.84 ± 16.24

Table 2.4 Fading corrected equivalent doses (Gy) for IRSL at 50°C (IR_{50}) and Post-IR IRSL at 225°C ($pIRIR_{225}$), and G-values for GOC-10 and MEND-06; fading corrected ages obtained from the IR_{50} are also shown.

Dose recovery tests

Dose recovery tests were conducted for each protocol to determine the ability of the protocol to recover a known dose of ~130 Gy.

Higher temperature protocol: pIRIR$_{290}$

Initially, four aliquots of two samples (GOC-01 and PTA-02) were set on a windowsill for three sunny days (based on Murray et al., 2013). Each aliquot was given ~130 Gy, then split by sample between the protocols outlined in Table 2.2, so that two aliquots per sample were measured using either protocol (results from pIRIR$_{225}$ discussed below). After subtracting residual doses obtained using the pIRIR$_{290}$ (discussed above), from the pIRIR$_{290}$ equivalent doses, ratios of the recovered to given dose were calculated (Figure 2.8a). All ratios fall below one (unity desired), with values of 0.72 ± 0.03 and 0.78 ± 0.03 for PTA-02, and 0.72 ± 0.03 and 0.75 ± 0.03 for GOC-01.

Lower temperature protocol: pIRIR$_{225}$

To test shorter bleaching durations, additional samples, and for comparison of the two protocols, two aliquots of GOC-10 and two aliquots of MEND-06 were set on a sunny windowsill for 24 h, dosed with ~130 Gy, and measured using the pIRIR$_{225}$ protocol. Residual doses obtained using the pIRIR$_{225}$ (discussed above) were subtracted from the equivalent doses for each sample, save for MEND-06 (due to extremely high error associated with the residual dose levels; Table 2.3 & Fig. 2.7a), to calculate ratios of the recovered to given doses (Fig. 2.8b). Ratios from PTA-02 and GOC-10 both fall below one, with values of 0.91 ± 0.03 and 0.95 ± 0.05 for PTA-02, and values of 0.70 ± 0.05 and 0.91 ± 0.03 for GOC-10. The ratios from GOC-01 and MEND-06 both split unity (the value of one), with values of 0.97 ± 0.03 and 1.10 ± 0.03 for GOC-01; and values of 1.09 ± 0.03 and 0.92 ± 0.03 for MEND-06 (recall residuals not

subtracted). Note that for the two samples measured with both protocols (PTA-02 and GOC-01), the dose recovery ratios measured with the $pIRIR_{225}$ fall closer to unity.

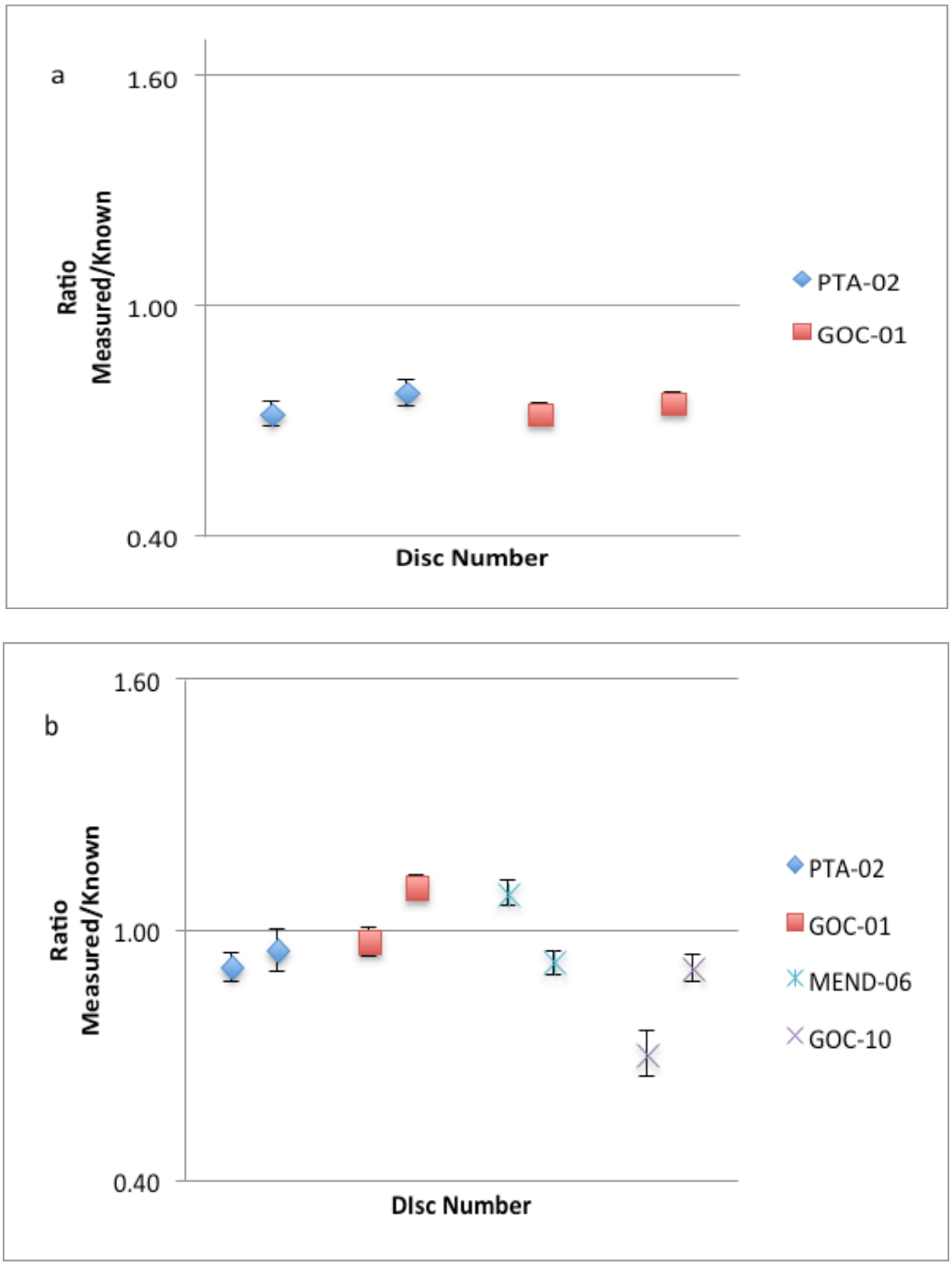

Figure 2.8 a) Dose recovery results from the $pIRIR_{290}$ protocol with a given dose of ~130 Gy; each point represents a single aliquot. Errors confined within data points. b) Dose recovery results from the $pIRIR_{225}$ protocol with a given dose of ~130 Gy; each point represents a single aliquot. Errors not confined within data points are represented with bars.

Marine terrace sediment age estimates

The ages of the sediment determined by the higher temperature protocol ($pIRIR_{290}$) are shown in Table 2.5. Residual doses were subtracted from PTA-02 and GOC-01, but no fading rates were applied to determine the best ages. The uncorrected equivalent dose values for all samples obtained via the $pIRIR_{290}$ range from 136.33 ± 10.30 Gy to 190.16 ± 22.49 Gy. These give an uncorrected age range of 49.90 ± 4.83 ka to 62.57 ± 4.79 ka. Using the $pIRIR_{290}$ protocol, residual dose levels were determined for PTA-02 and GOC-01. These values were subtracted from the uncorrected equivalent dose values for each sample, yielding a corrected equivalent dose from which corrected ages were calculated. The corrected age of the sediment from PTA-02 is 50.91 ± 7.49 ka, determined from seven aliquots; and from GOC-01 is 52.47 ± 3.87 ka, determined from seven aliquots. The best age that was determined for each sample using the $pIRIR_{290}$ protocol is shown in Table 2.5. Where residual doses are available, they were subtracted; otherwise the best age was determined from the uncorrected equivalent dose values. No additional ages were determined using this temperature protocol due to the poorer performance of the sediment with this protocol during dose recovery tests, and the higher residual dose levels (see above).

Table 2.5 Summary of results from $pIRIR_{290}$ for uncorrected D_e values (Gy), uncorrected ages (ka), and corrected ages (ka).

Sample	No. of aliquots	D_e uncorrected (Gy)	Uncorrected ages (ka)	Corrected ages[a] (ka)	Best age[b] (ka)
GOC-01	n=7	154.51 ± 6.07	56.55 ± 4.07	52.47 ± 3.87	52.47 ± 3.87
GOC-02	n=9	136.33 ± 10.30	49.90 ± 4.83		49.90 ± 4.83
PTA-01	n=4	190.16 ± 22.49	58.66 ± 7.66		58.66 ±7 .66
PTA-02	n=7	189.80 ± 9.52	62.57 ± 4.79	50.91 ± 7.49	50.91 ± 7.49

[a]Age correction done by subtracting residual dose levels.
[b]Best age determined for each sample.

The ages of the sediment determined by the lower temperature protocol ($pIRIR_{225}$) are shown in Table 2.6. The uncorrected equivalent dose values for all samples obtained via the $pIRIR_{225}$ range from 108.75 ± 3.36 Gy to 142.09 ± 6.32 Gy. These data give an uncorrected age range of 39.80 ± 2.70 ka to 54.35 ± 2.56 ka. Using the $pIRIR_{225}$, residual dose levels were measured for samples GOC-01, GOC-10, PTA-02, and MEND-06. The residual dose values were subtracted from the uncorrected equivalent dose values for samples GOC-01 and PTA-02; which yield corrected ages of 38.09 ± 2.61 ka and 38.36 ± 2.66 ka, respectively. The residual dose value for GOC-10 was subtracted from the uncorrected equivalent dose value. As fading rates were not applied, the best age (corrected for residual dose levels only) is 46.25 ± 2.70 ka. The residual dose value obtained for MEND-06 is 58.59 ± 36.62 Gy (Table 2.3). The uncertainty on this value is markedly high, thus the residual dose has not been subtracted from the uncorrected equivalent dose value due to the extreme error. As fading rates were low, they were not applied to the uncorrected equivalent dose value, which yielded a best age of 54.35 ± 2.56 ka for MEND-06. The best age that was determined for each sample is presented in Table 2.6.

Table 2.6 Summary of results from $pIRIR_{225}$ for uncorrected D_e values (Gy), uncorrected ages (ka), and corrected ages.

Sample	No. of aliquots	D_e uncorrected (Gy)	Uncorrected ages (ka)	Corrected ages[a] (ka)	Corrected ages[b] (ka)	Corrected ages[c] (ka)	Best age[d] (ka)
GOC-01	n=24	108.75 ± 3.36	39.80 ± 2.70	38.09 ± 2.61			38.09 ± 2.61
GOC-10	n=26	112.64 ± 3.62	49.66 ± 2.82	46.25 ± 2.70	54.63 ± 3.89	51.21 ± 6.18	46.25 ± 2.70
GOC-12	n=2	119.44 ± 4.97	48.39 ± 3.45				48.39 ± 3.45
PTA-02	n=24	134.49 ± 4.40	44.33 ± 2.94	38.36 ± 2.66			38.36 ± 2.66
PTA-06	n=22	142.09 ± 6.32	43.83 ± 3.11				43.83 ± 3.11
MEND-06	n=23	111.56 ± 3.47	54.35 ± 2.56	25.80 ± 17.94	65.21 ± 3.41	36.66 ± 48.29	54.35± 2.56

[a]Age correction done by subtracting residual dose levels.
[b]Age correction done by applying fading rates only.
[c]Age correction done by subtracting residual dose levels and applying fading rates.
[d]Best age determined for each sample.

Discussion

OSL protocols

Based on the dose recovery test results (not showing unity, Fig. 2.8a) and the higher residual dose levels observed from the higher temperature protocol (Fig. 2.6; Table 2.3), it was determined that the $pIRIR_{290}$ was not the most appropriate protocol for these deposits. The $pIRIR_{225}$ protocol performed more favorably, with dose recovery tests close to unity (Fig. 2.8b) and mostly lower residual dose levels (Figs. 2.6 & 2.7, Table 2.3). Roberts (2012) conducted a test of these protocols and also found the $pIRIR_{290}$ protocol gave age overestimates, and that lower temperature protocols (from 225 to 270°C) yielded ages that were in agreement with independent age controls. Residual dose levels for MEND samples were not measured using the $pIRIR_{290}$, and were notably higher than those observed for the PTA and GOC samples that were measured using the $pIRIR_{225}$ protocol. The reason for this is unclear, and it is recognized that perhaps neither protocol is well suited to measure the residual dose levels of these particular deposits.

Thomsen et al. (2008) was first to show how the pIRIR method minimized fading rates, especially when compared to the traditional IR measurement generally made at 50°C (with no subsequent measurement). They demonstrated fading rates of ~0.5-1.5%/decade for the $pIRIR_{225}$ method (250°C 60s preheat) and rates of ~1.5-3.5%/decade for the IR_{50}. Buylaert et al. (2009) tested the $pIRIR_{225}$ protocol and found similarly low fading rates, (1.62 ± 0.06%/decade). In her investigation of the pIRIR method with various IRSL stimulation and preheat temperature, Roberts (2012) also conducted fading tests of the pIRIR method and the IR50. The pIRIR fading rate she observed was ~1-1.5%/decade, and ~4%/decade observed for the conventional IR_{50}. Our

fading rates of ~5 %/decade for the IR_{50} measurement, and ~2 %/decade for the $pIRIR_{225}$ are similar to those observed in literature, though ours seems slightly higher on both accounts.

Terrace deposits

Though it is assumed that the sands studied presently are marine deposits, a detailed sedimentology study of the terrace deposits at each location is recommended as future work to better interpret the results. The origin of the sands affects the depositional complexity of the area, as well any post-depositional events. As such, various interpretations assuming marine sand or nonmarine sand are discussed below.

Scenarios for marine deposits

If the sands were determined to be marine in origin, then one interpretation of our data is that they were deposited on the terrace shortly after the terrace was cut, during MIS 3. Figure 2.9 illustrates a global context for this interpretation showing the age for PTA-terrace plotted along a eustatic sea-level curve (modified from Muhs et al., 2012). Though most studies agree that the PTA-terrace was cut during the 80 ka interglacial high stand, the interpretation is not without ambiguity. OSL of quartz by Spencer in 2008 (unpublished) investigated the PTA-terrace at Point Arena, Tomales Bay, and Green Oaks Creek (Fig. 2.1) and yielded ages of ca. 40,000 yr B.P. Perg et al. (2001) were the first to apply cosmogenic radionuclides (CRNs) to sandy deposits with well-developed soils, and did so to date a flight of five terraces along the California coast, immediately north of Santa Cruz (Fig. 2.1). They found the youngest terrace (identified as the Santa Cruz terrace) to be ca. 58 ka, and correlated it with the MIS 3 high stand. Grove et al. (2010) conducted luminescence dating on the lowest terrace platform at Point Reyes (Fig 2.1). Using quartz OSL, TL, and feldspar IRSL, they obtained an age using each method for five locations, though they found the IRSL to be most accurate. The best sites were interpreted as cut

during MIS 4 (~65 ka) and MIS 5a (~80 ka), though another site also gave an age in MIS 3 (~45 ka).

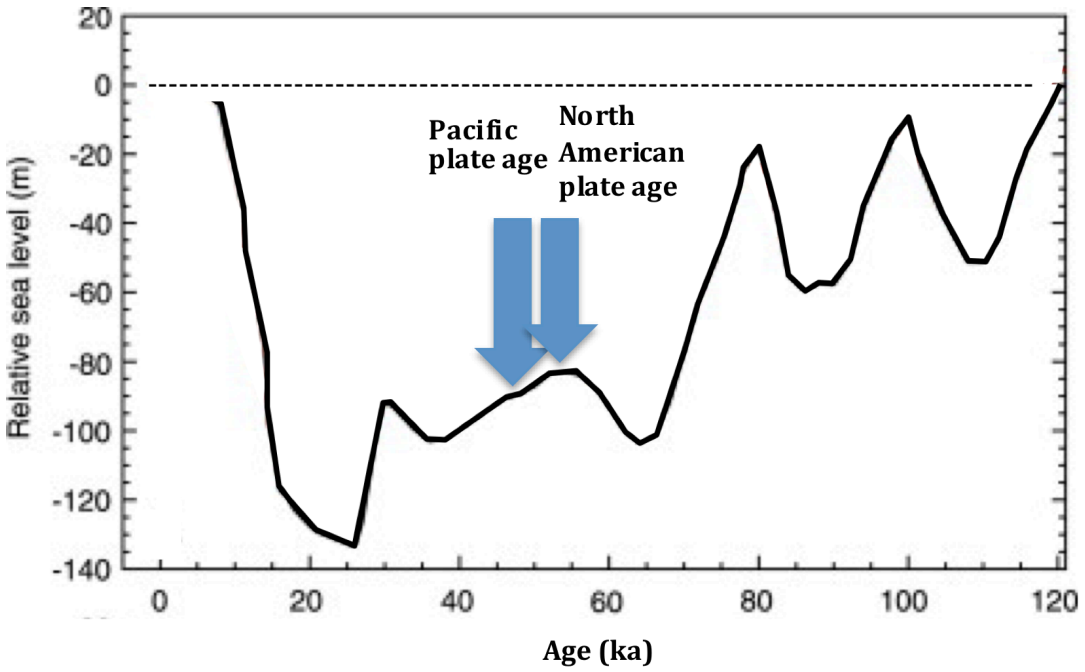

Figure 2.9 **Ages for PTA-terraces from the Pacific plate and North America plate plotted on an eustatic sea-level curve, modified from Muhs et al. 2012. Errors are approximately within the arrow width. Note that some relative sea levels differ from formation altitudes listed in Table 2.7.**

If the terrace was only ~45,000 years old, then the slip rates would be ca. 29-40 mm/yr (4-15 mm/yr faster than slip rates calculated by Prentice, 1989). Though DeMets et al., (1987) proposed a slip rate for the Pacific-North American plate motion of 46-51 mm/yr, it is more likely that the "lost" stress is compensated in splays to the SAF, and fault-normal compression (Prentice, 1989), than by significantly higher slip rates. Additionally, the MIS 3 high stands ranged from 29-37 meters below the sea level today (Table 2.7), which would greatly affect uplift rates. The PTA-terrace at Point Arena is approximately 26 m above sea level, meaning the uplift rates for the terrace if cut during MIS 3 would be approximately 1.4-1.6 mm/yr - more than three times the 0.25 and 0.49 mm/yr calculated by Prentice (1989) for this and the surrounding area.

Table 2.7 Sea levels and corresponding MIS stage and altitude as compared with modern sea level. Modified from Prentice (1989); ages compiled by Bull (1985) from Bloom et al. (1974) and Chappell (1983).

MIS Stage	Age (ka)	Altitude formed (meters)
3A	40	-37
3B	46	-37
3C	57	-29
3D	64	-26
4A	76	-46
5A	83	-13

An alternative interpretation of our data for these marine sands is that they have been disturbed since initial deposition, causing a more recent resetting of the luminescence signal. Resetting could have been due to a geomorphic event occurring ca. 35,000 yrs ago that was significant enough to rework the sands and effectively bleach the sediment, or the event could be significant disturbance via bioturbation. In this scenario, it is assumed that the terrace was cut during the 80 ka high stand and followed the model from Bradley and Griggs (1976) as discussed earlier. Bradley and Griggs (1976) also discuss a similar situation in which they found marine deposits upon the Davenport platform (a component of the Santa Cruz terrace), to be much younger than the platform itself, and concluded they were deposited by subsequent and multiple regressions. This scenario seems to be a credible fit for the OSL results, previous U-series ages, and field observations. It is important to note that with this interpretation, an OSL approach would not yield the age of the terrace, but the timing of the subsequent reworking event. Across literature, a parallel can be drawn to connect the lowest terrace at Davenport/Santa Cruz (Bradley and Griggs, 1976; Kennedy et al., 1982; Muhs et al. 2003), Point Ano Nueavo (Muhs et al., 2003), Green Oaks Creek (Muhs et al., 2003), Point Reyes Peninsula (Grove et al., 2010), Point Arena (Muhs et al., 1990, 1994, 2002; Kennedy et al., 1982) as having all been cut during the 80

ka high stand (Fig. 2.1). If this is the same terrace along each of these points, then it may be important to note that such reworking events may not be localized to the present sites, but might have occurred extensively along the California coast.

Interpretations for nonmarine deposits

If the sands were determined to be nonmarine in origin, and if one accepts that the PTA-terrace was cut ~80,000 yrs ago, then an interpretation of the data could be that there is an unconformity present. Approximately 45,000 year-old nonmarine sands are directly atop an approximately 80,000 year-old terrace platform, implying that ~35,000 years of geologic record is missing. In this scenario, the marine sand would have been completely eroded. Grove et al. (2010) suggest that the marine sand north of Point Reyes has been eroded and the platform is now overlain by ~30 m of alluvial sediment, though they do not imply that an unconformity is present. This statement would only affect PTA and MEND sampling sites, as GOC is located south of Point Reyes (Fig. 2.1). However, this scenario is not in agreement with field observations for PTA as the prominent fossil bed that occurs at GOC (Fig. 2.3) also outcrops at PTA, and is comprised of marine fossils. The argument for an unconformity at Mendocino is stronger as the fossil layer has not been found there; however, it would be complex indeed if an unconformity occurred only at this site, and not the others.

Age Correlation

Though the origin of the sand introduces various interpretations, it is still relevant that the OSL analysis of the sands at each locality and across the fault give rise to similar ages. A two-tailed t-test comparing uncorrected ages for the Pacific plate obtained via the $pIRIR_{225}$ protocol and the uncorrected age for MEND-06 on the North American plate shows the age difference is significant, though specific t-tests comparing GOC-10 to MEND-06, and GOC-12 to MEND-06

show they are statically the same. A two-tailed t-test comparing the uncorrected ages for the Pacific plate obtained via the $pIRIR_{290}$ protocol and the uncorrected age for MEND-06 also shows they are statistically the same. Though no fossils have been found to offer an age control at Mendocino, this work has shown that a correlation can be made based on the sediment age. If it could be demonstrated that older and higher terraces also yield corresponding (older) ages across the fault, then using OSL to date the sediment mantling marine terraces could be an effective correlation tool. As such, a correlation is drawn from the PTA-terrace at the locations of Point Arena and Green Oaks Creek on the Pacific plate, southwest of the SAF, to the PTA-terrace at Mendocino on the North American plate, northeast of the SAF. This correlation reinforces the offset of 1.3 km - 1.8 km of the PTA-terrace, mapped by Prentice and Kelson (2006) (Fig. 2.2); and, the accuracy of the slip rates (despite the age of the terrace) is improved.

Summary and Conclusion

Three sites were sampled along a marine terrace offset by the northern San Andreas Fault, and analyzed using a contemporary OSL method, termed the pIRIR technique. Two temperature regimes were used to test the applicability of each pIRIR protocol for the sediment, and to determine the age of the sediment mantling on the terrace. From dose recovery tests and residual dose levels, it appears the higher temperature protocol is not well suited to date these sediments. The lower residual dose levels, dose recovery tests resulting closer to unity, and diminished fading observed via the $pIRIR_{225}$ proved the lower temperature protocol a more appropriate dosimeter for these samples, and gave rise to ages ranging from 38.36 ± 2.66 to 54.63 ± 3.89 ka. It is assumed that this range does not represent the age of the terrace, but instead the age of the most recent deposition or reworking event of the sediment. A detailed sedimentology study and an investigation of the sediment mantling higher terraces are

recommended as future work in this area. While the origin of the sediment is currently unclear, the similarity of the ages across the fault is significant and a correlation of the PTA-terrace from the Pacific plate to the North American plate works to affirm the offset distance due to SAF motion. Though it seems unlikely that the pIRIR technique can be used to determine the age of marine terraces, OSL analysis of marine terrace deposits may prove to be a reliable correlation tool.

Chapter 3 - Summary and Conclusions

The field of OSL dating has experienced significant progress over the past decades, and continues to evolve with the development of new protocols and improvements to older methods. The pIRIR approach is at the forefront of feldspar advancements, nearly mitigating the need to account for fading. This work adds to the existing knowledge base of the pIRIR method; namely, that the lower temperature protocol ($pIRIR_{225}$) was better suited for the sediments than the higher temperature protocol ($pIRIR_{290}$). This was determined through the application of these protocols to sediments deposited on the Point Arena terrace, with the objectives to date them via OSL, and to correlate the terrace across the San Andreas Fault. The age determined for the sediment is ca. 35,000 years younger than the more widely accepted terrace age of ca. 80,000 years. This discordance requires alternative data interpretations, and calls attention to the origin of the sediment. Nonmarine sediment would not present a significant problem, as the deposits would obey superposition; however, field observations imply that the deposits are marine sand. Nonetheless, the OSL results, which suggest correlation of the Point Arena terrace across the fault even without demonstrating U-series age concordance, reveal an alternative capacity of OSL as a useful correlation tool.

References

Adamiec, G., Aitken, M., 1998. Dose-rate conversion factors: update. Ancient TL 16, 37–50.

Auclair, M., Lamothe, M., Huot, S., 2003. Measurement of anomalous fading for feldspar IRSL using SAR. Radiation Measurements 37, 487-92.

Bloom, A.L., Broecker, W.S., Chappell, J., Matthews, R.K., Mesolella, K.J., 1974. Quaternary sea-level fluctuations on a tectonic coast: New $^{230}Th/^{234}U$ dates from the Huon Peninsula, New Guinea. Quaternary Research 4, 185-205.

Bradley, W.C., Griggs, G.B., 1976. Form, genesis, and deformation of central California wave-cut platforms. Geological Society of America Bulletin 87, 433-39.

Bull, W.L., 1985. Correlation of flights of global marine terraces. Tectonic Geomorphology, M. Morisawa and J. Hack, eds., Binghamton Symposia in Geomorphology, International Series 15, 129-52.

Buylaert, J.P., Jain, M., Murray, A.S., Thomsen, K.J.,Thiel, C.,Sohbati, R., 2012. A robust feldspar luminescence dating method for middle and Late Pleistocene sediments, Boreas 41, 435-51.

Chappell, J.M., 1983. A revised sea-level record for the last 300,000 years from Papua New Guinea. Search 14, 99-101.

DeMets, C., Gordon, R.G., Stein, S., Argus, D.F., 1987. A revised estimate of Pacific-North America motion and implications for western North America plate boundary zone tectonics. Geophys. Res. Letters 14, 911-14.

Duller, G. A. T., Wintle, A. G. & Hall, A. M., 1995. Luminescence dating and its application to key pre-Late Devensian sites in Scotland. Quaternary Science Reviews 14, 495–519.

Fuchs, M., Owen, L.A., 2008. Luminescence dating of glacial and associated sediments: review, recommendations and future directions. Boreas 37, 636-59.

Galbraith et al., 1999. Optical dating of single and multiple grains of quartz from jinmium rock shelter, Northern Australian: Part 1, experimental design and statistical models. Archaeometry 41, 339-64.

Grove, K., Sklar, L.S., Scherer, A.M., Lee, G., Davis, J., 2010. Accelerating and spatially-varying crustal uplift and its geomorphic expression, San Andreas Fault zone north of San Francisco, California. Tectonophysics 496, 256-68.

Huntley, D.J., Godfrey-Smith, D.I., Thewalt, M.L.W., 1985. Optical dating of sediments. Nature 313, 105-07.

Huntley, D.J., Baril, M.R., 1997. The K content of K-feldspars being measured in optical dating or in thermoluminescence dating. Ancient TL 15, 11-13.

Hütt, G., Jaek, I., Tchonka, J., 1988. Optical dating: K-feldspars optical response stimulation spectra. Quaternary Science Reviews 7, 381-85.

Kennedy, G.L., Lajoie, K.R., and Wehmiller, J.F., 1982. Aminostratigraphy and faunal correlations of late Quaternary marine terraces, Pacific Coast, USA. Nature 299, 545–47.

Lukas, S., Spencer, J.Q., Robinson, R.A.J., Benn, D.I., 2007. Problems associated with luminescence dating of Late Quaternary glacial sediments in the NW Scottish Highlands. Quaternary Geochronology 2, 243-48.

Muhs, D.R., Kelsey, H.M., Miller, G.H., Kennedy, G.L., Whelan, J.F., McInelly, G.W., 1990. Age estimates and uplift rates for late Pleistocene marine terraces: southern Oregon portion of the Cascadia forearc. Journal of Geophysical Research 95, B5.

Muhs, D.R., Kennedy, G.L., Rockwell, T.K., 1994. Uranium-series ages of marine terrace corals from the Pacific coast of North America and implications for the last- interglacial sea level history. Quaternary Research 42, 72–87.

Muhs, D.R., Simmons, K.R., Kennedy, G.L., Ludwig, K.R., and Groves, L.T., 2002. A cool eastern Pacific Ocean at the close of the last interglacial period, ca. 80,000 yr B.P. Geological Society of America Abstracts with Programs, 34, 130.

Muhs, D.R., Prentice, C., Merritts, D.J., 2003. Marine terraces, sea level history and Quaternary tectonics of the San Andreas fault on the coast of California: *in* Easterbrook, D., ed., Quaternary Geology of the United States, INQUA 2003 Field Guide Volume, Desert Research Institute, Reno, NV, 1–18.

Muhs, D.R., Simmons, K.R., Schumann, R.R., Groves, L.T., Mitrovica, J.X., Laurel, D., 2012. Sea-level history during the Last Interglacial complex on San Nicolas Island, California: implications for glacial isostatic adjustment processes, paleozoogeography and tectonics. Quaternary Science Reviews 37, 1-25.

Murray, A.S., Wintle, A.G., 2000. Luminescence dating of quartz using an improved single-aliquot regenerative-dose protocol. Radiation Measurements 32, 57–73.

Murray, A.S., Olley, J.M., 2002. Precision and accuracy in the optically stimulated luminescence dating of sedimentary quartz: a status review. Geochronometria 21, 1-16.

Murray, A.S., Wintle, A.G., 2003. The single aliquot regenerative dose protocol: potential for improvements in reliability. Radiation Measurements 37, 57-73.

Murray, A.S., Buylaert, J.P., Thomsen, K.J., Jain, M., 2009. The effect of preheating on the IRSL signal from feldspar. Radiation Measurements 44, 554-59.

Murray, A.S., Schmidt, E.D., Stevens, T., Buylaert, J.-P., Markovic, S.B., Tsukamoto, S., Frechen, M., 2013. Dating Middle Pleistocene loess from Stari Slankamen (Vojvodina, Serbia) – Limitations imposed by the saturation behavior of an elevated temperature IRSL signal, Catena, http://dx.doi.org/10.1016/j.catena.2013.06.029

Perg, L.A., Anderson, R.S., Finkel, R.C., 2001. Use of a new ^{10}Be and ^{26}Al inventory method to date marine terraces, Santa Cruz, California, USA. Geology 29, 879-82.

Prentice, C.S., 1989, Earthquake geology of the northern San Andreas fault near Point Arena, California: Ph.D. thesis, California Institute of Technology, 252 p.

Prentice, C.S., and Kelson, K.I., 2006, The San Andreas fault in Sonoma and Mendocino counties, in Prentice, C.S., Scotchmoor, J.G., Moores, E.M., and Kiland, J.P., eds., 1906 San Francisco Earthquake Centennial Field Guides: Field trips associated with the 100th Anniversary Conference, 18–23 April 2006, San Francisco, California: Geological Society of America Field Guide 7, p. 127–156, doi: 10.1 130/2006.1906SF(11).

Prescott, J.R., Hutton, J.T., 1994. Cosmic ray contributions to dose rates for luminescence and ESR dating: large depths and long-term time variations. Radiation Measurements 23, 497–500.

Rittenour, T.M., 2008. Luminescence dating of fluvial deposits: applications to geomorphic, palaeoseismic and archaeological research. Boreas 37, 613-35.

Rhodes, E.J., 2011. Optically Stimulated Luminescence Dating of Sediments over the past 200,000 years. Annu. Rev. Earth Planet. Sci. 39, 461-88.

Roberts, H.M., 2012. Testing Post-IR IRSL protocols for minimizing fading in feldspars, using Alaskan loess with independent chronological control. Radiation Measurements 47, 716-24.

Spencer, J.Q., Owen, L.A., 2004. Optically stimulated luminescence dating of Late Quaternary glaciogenic sediments in the upper Hunza valley: validating the timing of glaciation and assessing dating methods. Quat. Sci. Rev. 23, 175-91.

Spencer, J.Q., Prentice, C.S., DeLong, S., 2008. Quartz Optically Stimulated Luminescence Dating of northern California marine terraces. Unpublished.

Spooner, N.A., 1992. Optical dating: Preliminary results on the anomalous fading of luminescence from feldspars. Quaternary Science Reviews 11, 139-45.

Spooner, N.A., 1994. The anomalous fading of infrared-stimulated luminescence from feldspars. Radiation Measurements 23, 625-32.

Thiel, C., Buylaert, J.P., Murray, A.S., Terhorst, B., Hofer, I., Tsukamoto, S., Frenchen, M., 2011. Luminescence dating of the stratzing loess profile (Austria) – Testing the potential of an elevated temperature post-IR IRSL protocol. Quat. Int. 234, 23-31.

Thomsen, K.J., Murray, A.S., Jain, M., Bøtter-Jenson, L., 2008. Laboratory fading rates of various luminsecnece signals from feldspar-rich sediment extracts. Radiation Measurements 43, 1474-86.

Thomsen, K.J., Murray, A.S., Jain, M., 2011. Stability of IRSL signals from sedimentary K-feldspar samples. Geochronometria 38, 1-13.

Wintle, A.G., 1973. Anomalous fading of thermoluminescence in mineral samples. Nature 243, 143-44.

Wintle, A.G., Murray, A.S., 2006. A review of quartz optically stimulated luminescence characteristics and their relevance in single-aliquot regeneration dating protocols. Radiation Measurements 41, 369-91.

Appendix A - Point Arena

The following is data appurtenant to the Point Arena study site that were obtained through this graduate work, but are not included in the manuscript of Chapter 2. Where n > 2, each figure represents an individual run and was compiled into a single radial plot; where n < 2, the growth curve for each disc is presented.

Higher temperature protocol ($pIRIR_{290}$) growth curves and radial plots

PTA-01

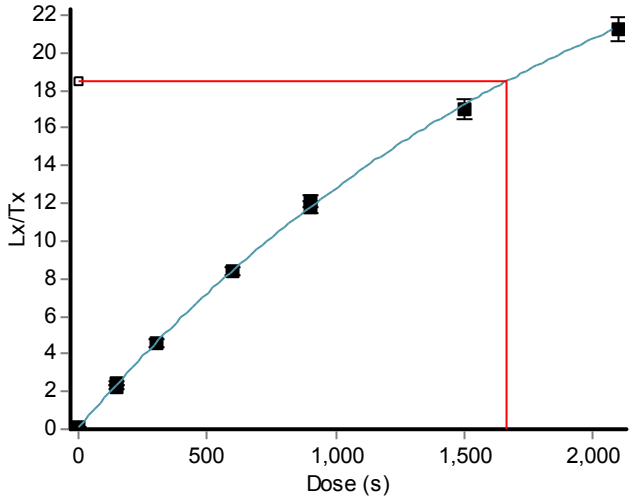

Figure A.3.1 PTA-01 growth curve, n=1.

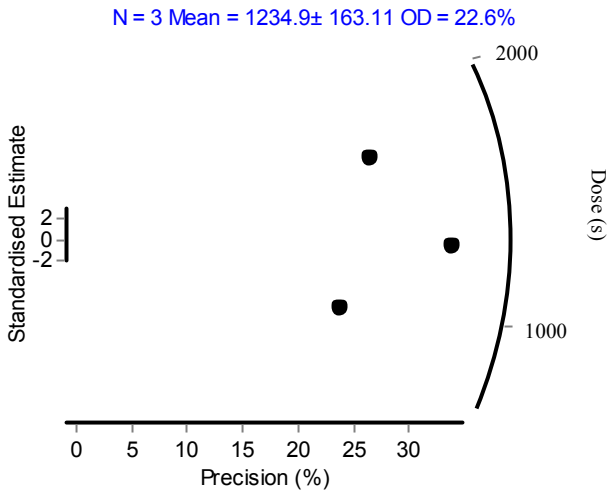

Figure A.3.2 PTA-01 radial plot; n=3.

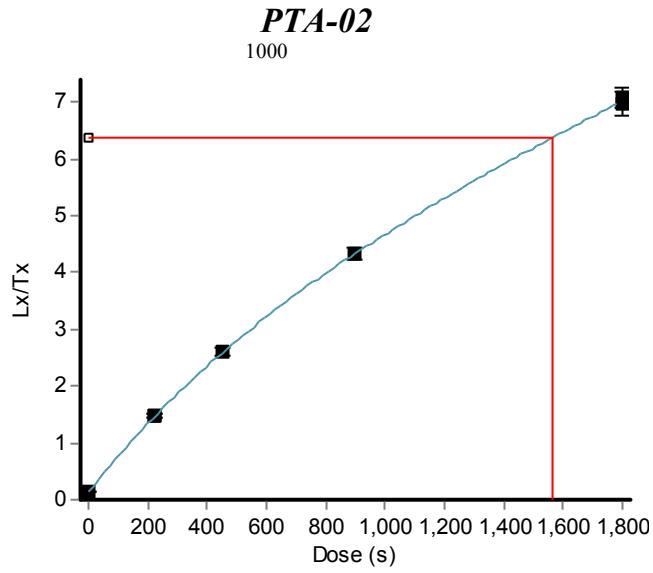

Figure A.3.3 PTA-02 growth curve; n=1.

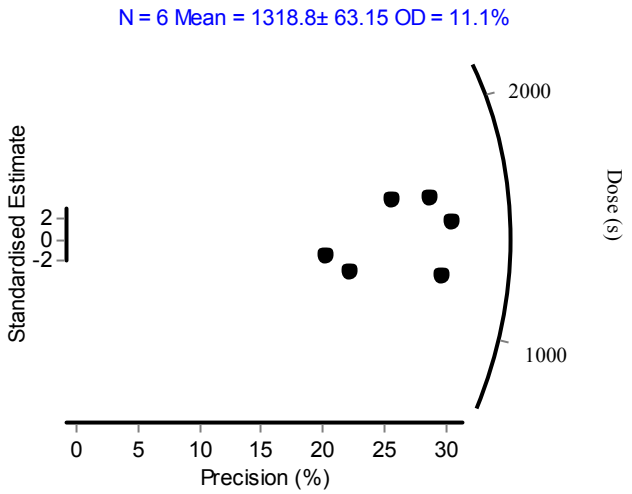

Figure A.3.4 PTA-02 radial plot; n=6.

Lower temperature protocol (pIRIR$_{225}$) growth curves and radial plots

PTA-02

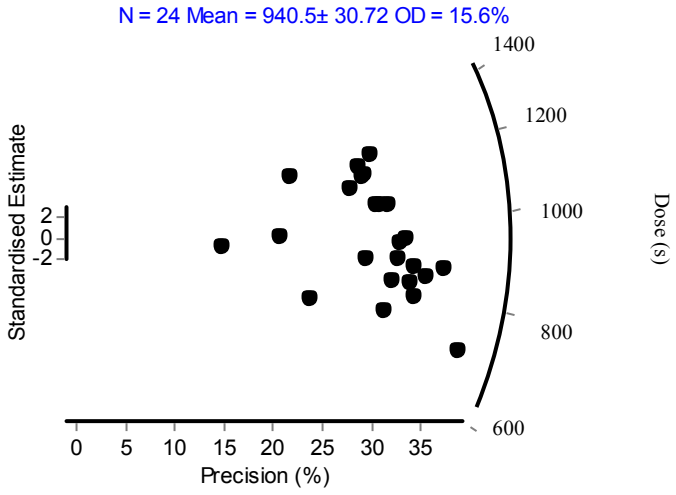

FigureA.3.5 PTA-02 radial plot; n=24.

PTA-06

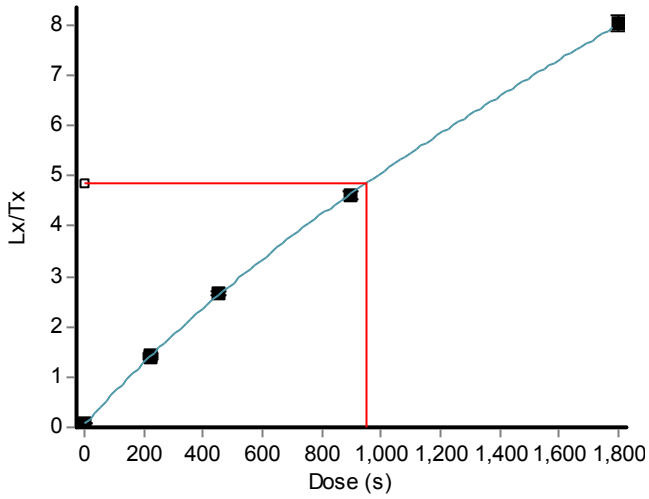

Figure A.3.6 PTA-06 growth curve; n=1.

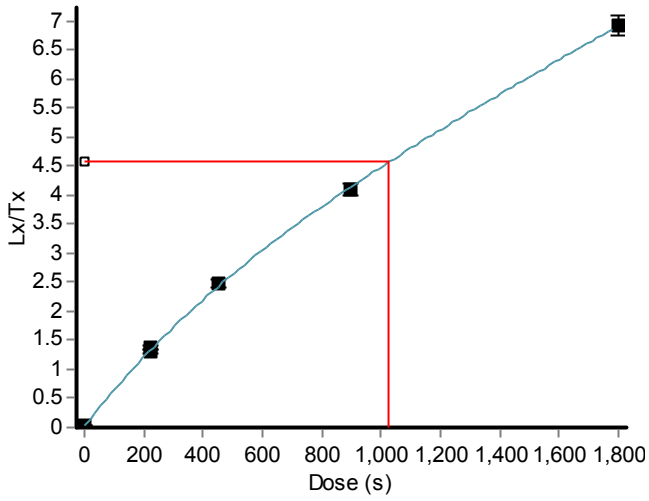

Figure A.3.7 PTA-06 growth curve; n=1.

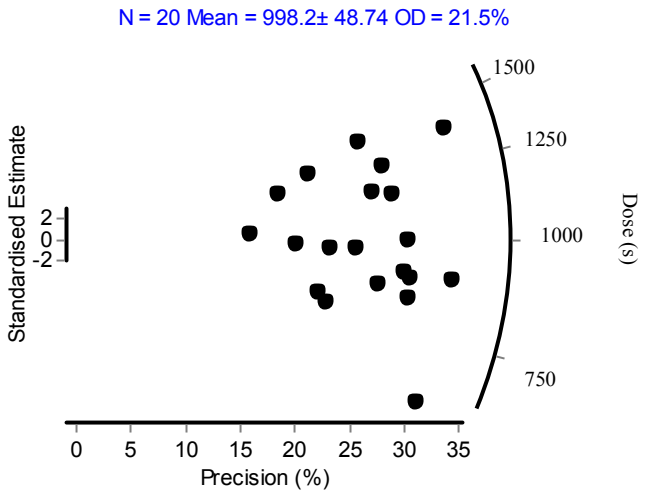

Figure A.3.8 PTA-06 radial plot; n=20.

Appendix B - Green Oaks Creek

The following is data appurtenant to the Green Oaks Creek study site that were obtained through this graduate work, but are not included in the manuscript of Chapter 2. Where n > 2, each figure represents an individual run and was compiled into a single radial plot; where n < 2, the growth curve for each disc is presented.

Higher temperature protocol ($pIRIR_{290}$) growth curves and radial plots

GOC-01

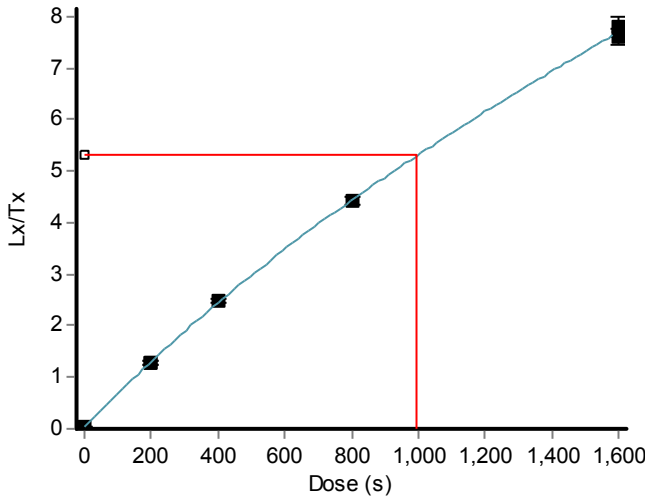

Figure B.3.9 GOC-01 growth curve; n=1

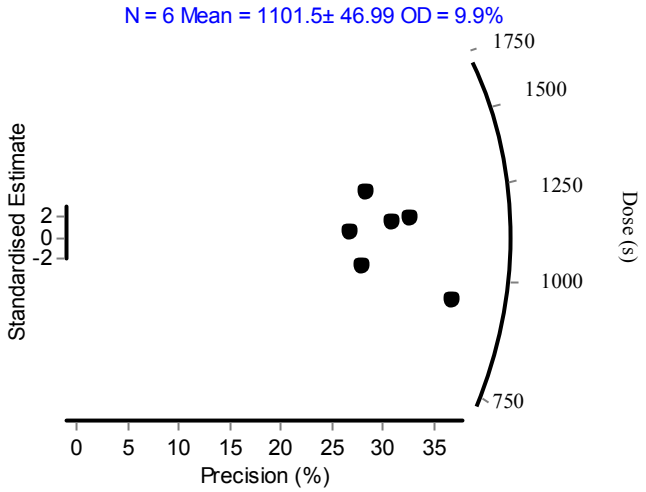

Figure B.3.10 GOC-01 radial plot; n=6.

GOC-02

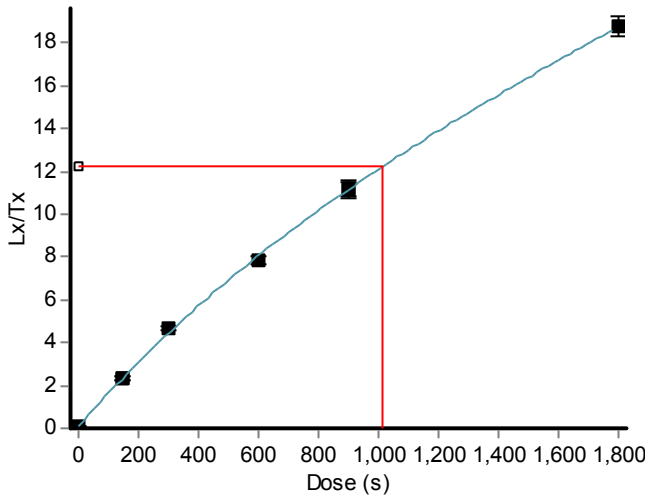

Figure B.3.11 GOC-02 growth curve; n=1.

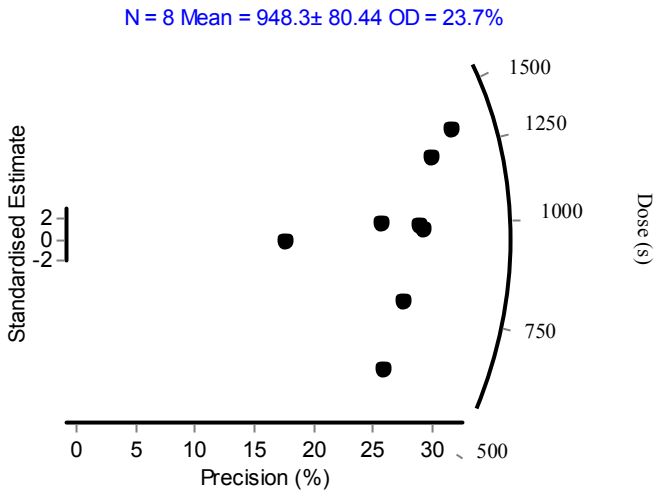

FigureB.3.12 GOC-02 radial plot; n=8.

Lower temperature protocol ($pIRIR_{225}$) growth curves and radial plots

GOC-01

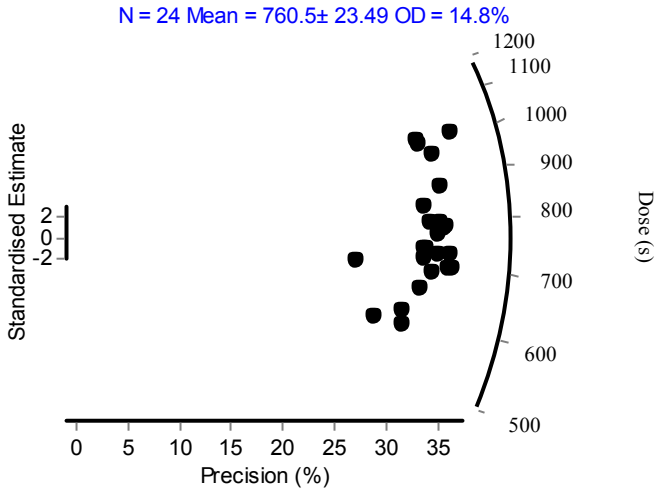

Figure B.3.13 GOC-01 radial plot; n=24.

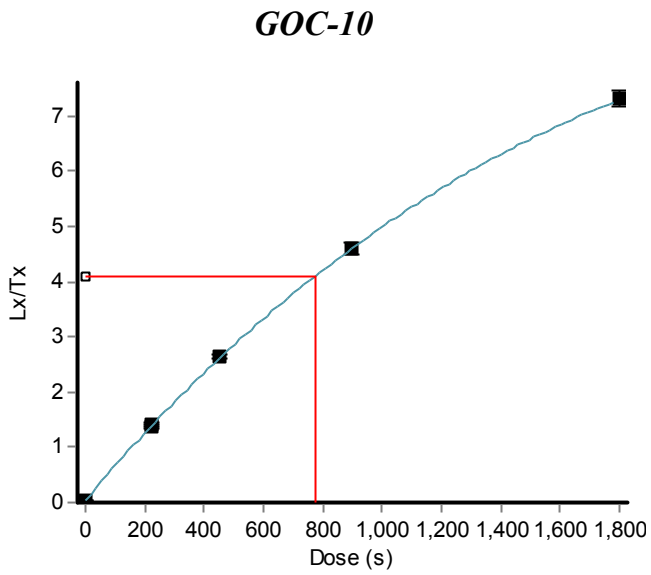

Figure B.3.14 GOC-10 growth curve; n=1.

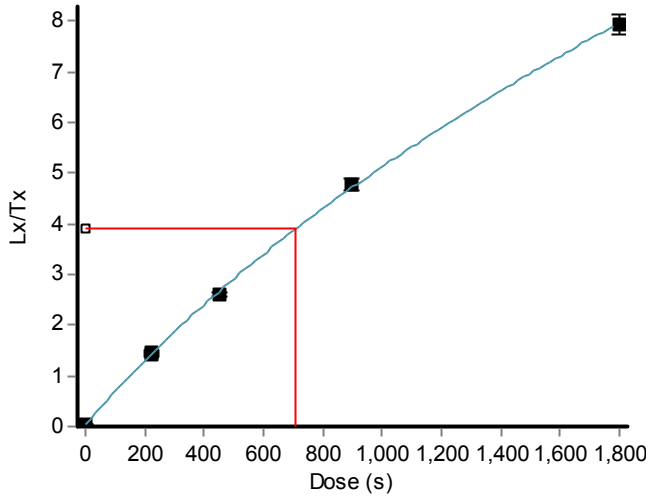

Figure B.3.15 GOC-10 growth curve; n=1.

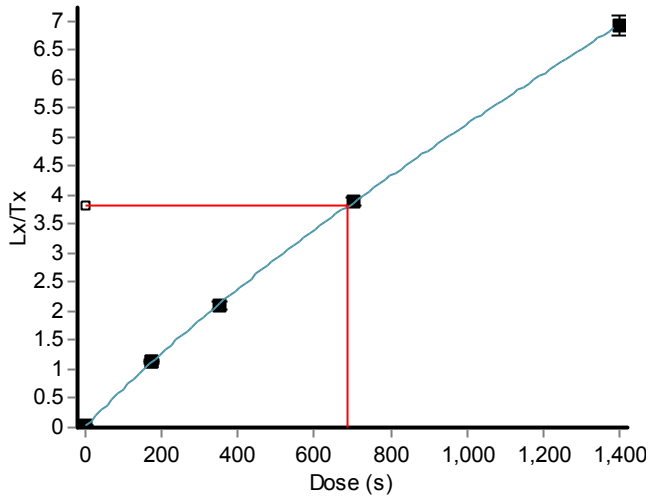

Figure B.3.16 GOC-10 growth curve; n=1.

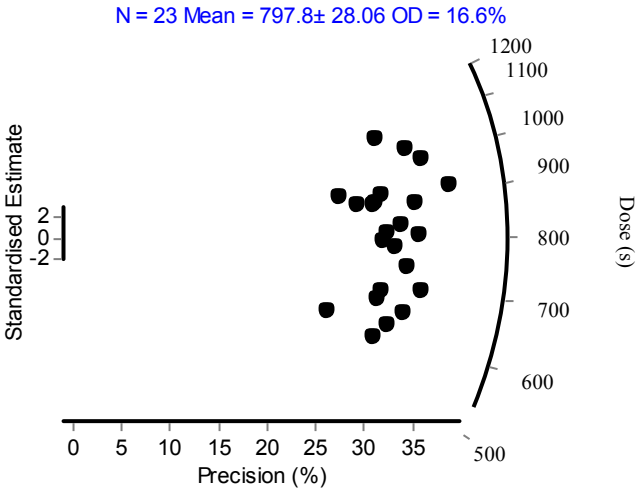

Figure B.3.17 GOC-10 radial plot; n=23.

GOC-12

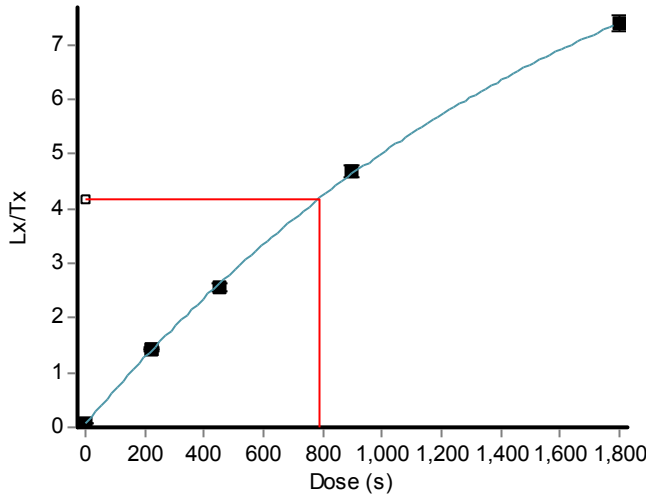

Figure B.3.18 GOC-12 growth curve; n=1.

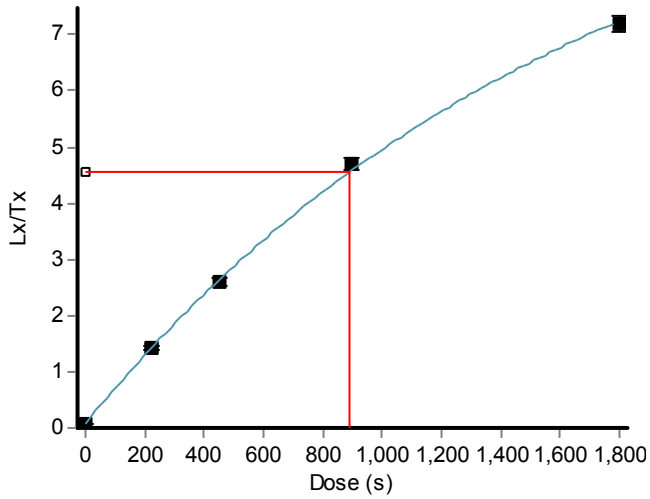

Figure B.3.19 GOC-12 growth curve; n=1.

Appendix C - Mendocino

The following is data appurtenant to the Mendocino study site that were obtained through this graduate work, but are not included in the manuscript of Chapter 2. Where n > 2, each figure represents an individual run and was compiled into a single radial plot; where n < 2, the growth curve for each disc is presented.

Lower temperature protocol ($pIRIR_{225}$) growth curves and radial plots

MEND-06

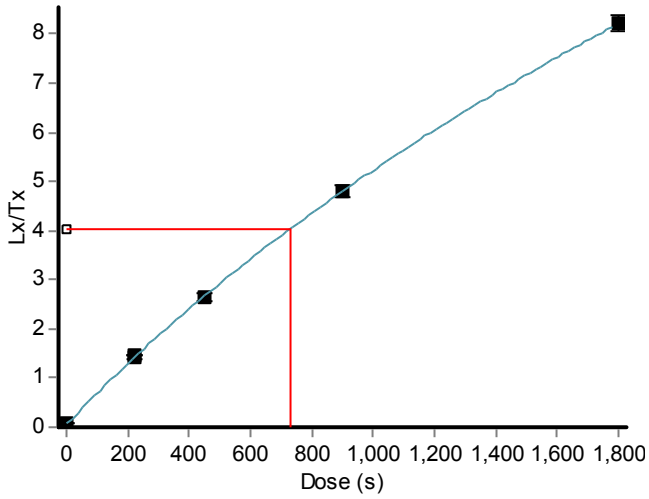

Figure C.3.20 MEND-06 growth curve; n=1.

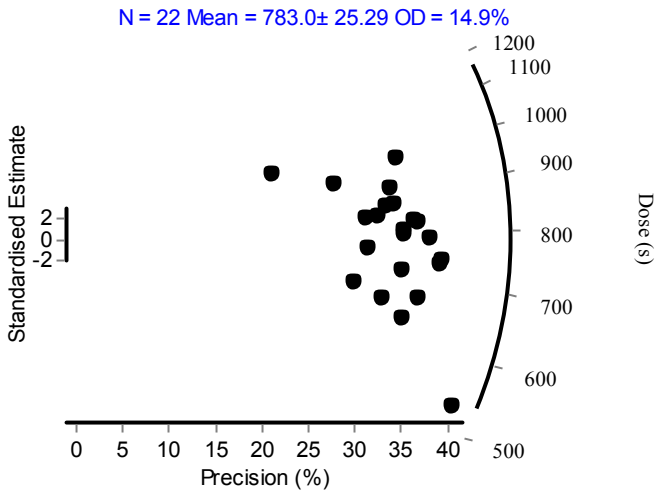

Figure C.3.21 MEND-06 radial plot; n=22.

Appendix D - Tomales Bay

The following is data appurtenant to the Tomales Bay study site (Tom's Point, TP), which was later suspected to be unrelated to the Point Arena terrace. Nonetheless, data were obtained through this graduate work from this site, and are presented below. Where n > 2, each figure represents an individual run and was compiled into a single radial plot; where n < 2, the growth curve for each disc is presented.

Higher temperature protocol ($pIRIR_{290}$) growth curves and radial plots

TP-01

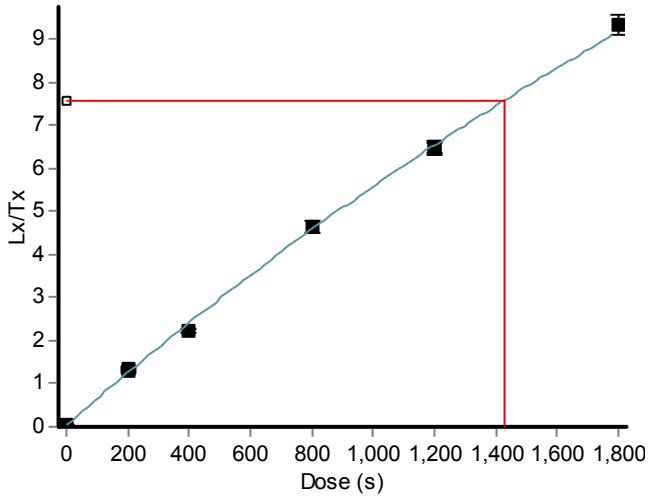

Figure D.3.22 TP-01 growth curve; n=1.

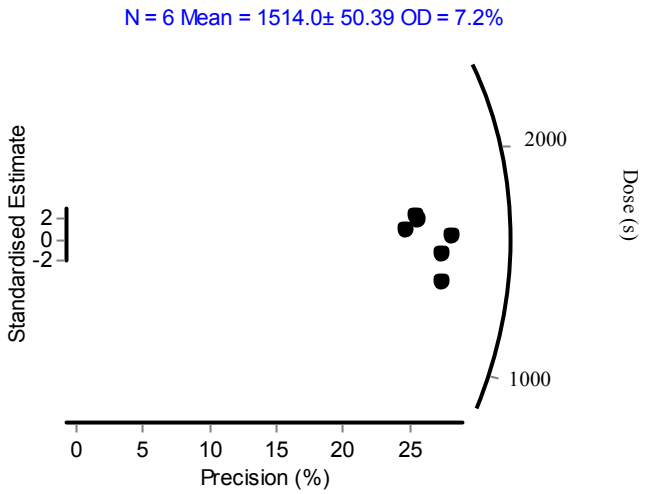

Figure D.3.23 TP-01 radial plot; n=6.